[Frontiers in Bioscience E2, 1028-1041, June 1, 2010]

AFM and fluorescence imaging of nanomechanical response in periodontal ligament cells

Liang Shi [1,2,3], Shenggen Shi[2], Jing Li[1], Quanmei Sun[1], Kai Feng[2], Peipei Chen[1], Shaoyan Si[2], Long Chen[1], Ye Li[2], Ping Dang[2], Chuhua Tang[2], Dong Han[1]

[1]Lab for Biological Imaging and Nanomedicine, National Center for Nanoscience and Technology, Beijing, 100190, China, [2]Department of Stomatology, 306 Hospital, Beijing, 100101, China, [3]Faculty of Stomatology, Capital University of Medical Sciences, Beijing, 100050, China

TABLE OF CONTENTS

1. ABSTRACT

Most biologists think that AFM has only a limited use in biological research due to its inability to study other than surface structures. Therefore, a BIO-AFM system has been developed to combine both AFM imaging and fluorescence detection, which acts as a powerful tool for a better understanding of dynamic cell processes. In this study, based on a custom-made BIO-AFM system, the elasticity and ultrastructure of living periodontal ligament cells (PDLCs) were investigated. The cantilever probe with a micron-sized bead was used to exert nano-loading force onto the PDLCs. The related signal of NO was then recorded simultaneously. The results show that PDLCs hold strong networks of stress fibers as well as high elastic modulus value, exhibiting the ability for better counteracting the external forces. In the mechano-transduction studies, an initial increase and subsequent drop in intracellular NO response was found. Furthermore, NO may diffuse from a stimulated cell to adjacent cells. In conclusion, our single-cell nano-mechanical study provides a significant advancement in elucidating the magnitude, location, time scale, and biomolecular mechanisms underlying cell mechano-transduction.

2. INTRODUCTION

Mechanical forces, such as compression- and shear forces, always act on cells *in vivo*, generating a trail of biochemical signals which further regulate a large number of physiological processes. By contrast, improper mechanical responses of cells may contribute to a variety of major human diseases (1). Therefore, responses of living cells to mechanical force have currently attracted tremendous attention in studies on cell biology, tissue engineering as well as pathophysiology (1-3).

Cells can sense mechanical stimuli via mechano-sensitive ion channels, integrin receptors, or tyrosine kinases (4-6). The exact mechanism involved and the downstream events may depend on both the type of stimulation and the degree of forces and is considered likely to involve cell- or tissue-specific components. An early and quasi-ubiquitous response to mechanical stimuli is increased intracellular concentration of calcium ions, which can be also transmitted to neighboring cells, thereby sensitizing a larger volume of tissue. The cytoskeleton is a closely interwoven network of actin, tubulin, and intermediate filaments that modulates cellular sensitivity to

mechanical stimuli by adapting its structure to accommodate prolonged mechanical strains (7, 8). Therefore, cytoskeletal integrity is highly important for the detection and transduction of mechanical strain (7, 9, 10).

The periodontal ligament cells (PDLCs) that exist between the cementum of the dental root and the alveolar bone, are exposed to mechanical stress all through their life, especially compression forces from occlusal pressure and orthodontic forces (11). The mechanical responses of the PDLCs may govern the homeostasis and remodeling of the periodontal ligament itself as well as repair and regeneration of other components of periodontal tissues, including resorption and formation of bone matrix during physiological and orthodontic tooth movement (12). Many previous studies have demonstrated that mechanical stress may induce expression in PDLCs of biological mediators, such as interleukin-6 (13), interleukin-1b (14-16), matrix metalloproteinases, metalloproteinase inhibitors (17), plasminogen activators (18), cyclooxygenase (COX)-2 (19, 20), alkaline phosphatase (21), type I collagen (22) and osteocalcin (23).

Recently, Araujo and colleagues employed the microarray analysis technology to assess gene expression profiles in three-dimensionally cultured PDLCs undercompression by a static force (24). The data showed that 108 of the 30,000 tested genes were differentially expressed following application of a mechanical force. Among them, 85 genes were up-regulated by mechanical stress, while 23 were down-regulated. The genes were involved in numerous biological processes, including communication, signaling, proliferation, stress response, and calcium ion release. A preceding study by Kanzaki and colleagues (25) proved that a static compressive force stimulates expression of receptor activator nuclear factor kB ligand (RANKL), a potent osteoclastogenic factor, via the induction of prostaglandin E2 (PGE2) by COX-2 activation in cultured PDLC monolayers. The PDLCs are now recognized as transformers of mechanical stress to biological signals in which a set of unique genes start to be expressed following auto-regulation. However, the precise mechanism whereby PDLCs convert mechanical signals to a biochemical response remains unclear. Mechano-transduction research at single cell levels is expected to be a suitable strategy to obtain a precise understanding of these mechanisms.

A number of different techniques have been used to apply strain to single cells, ranging from: poking with a micropipette (26, 27), pulling by magnetic micro-beads adhering on cell membrane in a magnetic field (28), driving by optical tweezers, substrate stretching (29), and exposure to hydrostatic pressure. These methods can be broadly divided into two categories: Those that apply stimulation over the whole cell (substrate stretch, fluid shear, intermittent hydrostatic pressure), and those that stimulate only a small part of the cell body (micro-bead pulling, micro-bead twisting, micropipette poking). But none of these techniques achieve a precise control of location and magnitude of the applied force.

In comparison to the methods mentioned, atomic force microscopy (AFM) enables a precise application of nano-Newton forces, precise measurement of cell elasticity (30), minimal cellular disruption (31), and determination of cellular strain distribution (32). Furthermore, by combining AFM with fluorescent microscopy, a much better understanding of the cellular signal regulation in response to mechanical force can be provided in real-time.

Since the invention in 1986 of AFM, it has been used as a nano-sensing tool to acquire 3-D information in real-space (33). When applied in biological research, it allows real-time imaging of living cells and tissues like blood vessel intima (34) in a physiological solution. The studies have resulted in a deeper understanding of cellular dynamic processes. Apart from offering high resolution images of cell surfaces, AFM has also been used to probe cellular mechanical properties (34-36), such as mechanical strain and elasticity, by analyzing the relationship between deflection of cells and the force applied to them.

In this present study, a custom-made combined system of AFM and inverted fluorescence microscopy was constructed as an integrated BIO-AFM unit. In this system, a micro-bead was attached to an AFM cantilever and used to exert a quantitative force on living cells. During the process a related fluorescent signal of nitric oxide (NO), marked by DAF-FM, was simultaneously recorded, enabling us to carry out nano-mechanics research on single cell levels.

3. METHODS AND MATERIALS

3.1. Cell culture

Human periodontal ligament cells (human PDLCs) were, with minor modifications, prepared in accordance with the method reported by Somerman and colleagues (37). The protocol for this experiment was reviewed and approved by the Capital Medical University (Beijing, China) Ethics Committee. Premolars extracted from healthy patients aged 12 to 36 years undergoing orthodontic treatment were washed twice with 0.01mol/l phosphate-buffered saline and tissue attached to the middle third of the root was removed. The coronal and apical portions of the root were cut to avoid contamination by cells from other tissues. The tissue was minced, placed in 35-mm tissue culture dishes (Corning, USA), and covered with sterilized glass cover slips. The medium used was a-minimal essential Eagle's medium (Hyclone, USA) supplemented with 100U/ml penicillin-G sodium, 100U/ml streptomycin sulfate, 0.25μg/ml amphotericin B (Gibco, USA), and 10% fetal calf serum (Hyclone, USA). The cultures were maintained at 37°C in a humidified 95% air and 5% CO_2. When the cells grew out from the explants and reached confluence, they were detached with 0.05% trypsin (Gibco) in phosphate-buffered saline for 10 min, and subcultured in culture flasks (Corning, USA). Some cells attached to the bottom of the flasks were discarded during serial passage to avoid contamination by epithelial cells, which are less easily detached than fibroblasts. The cells were then identified as described previously (38). The evidence from Phase-contrast imaging showed that cells at

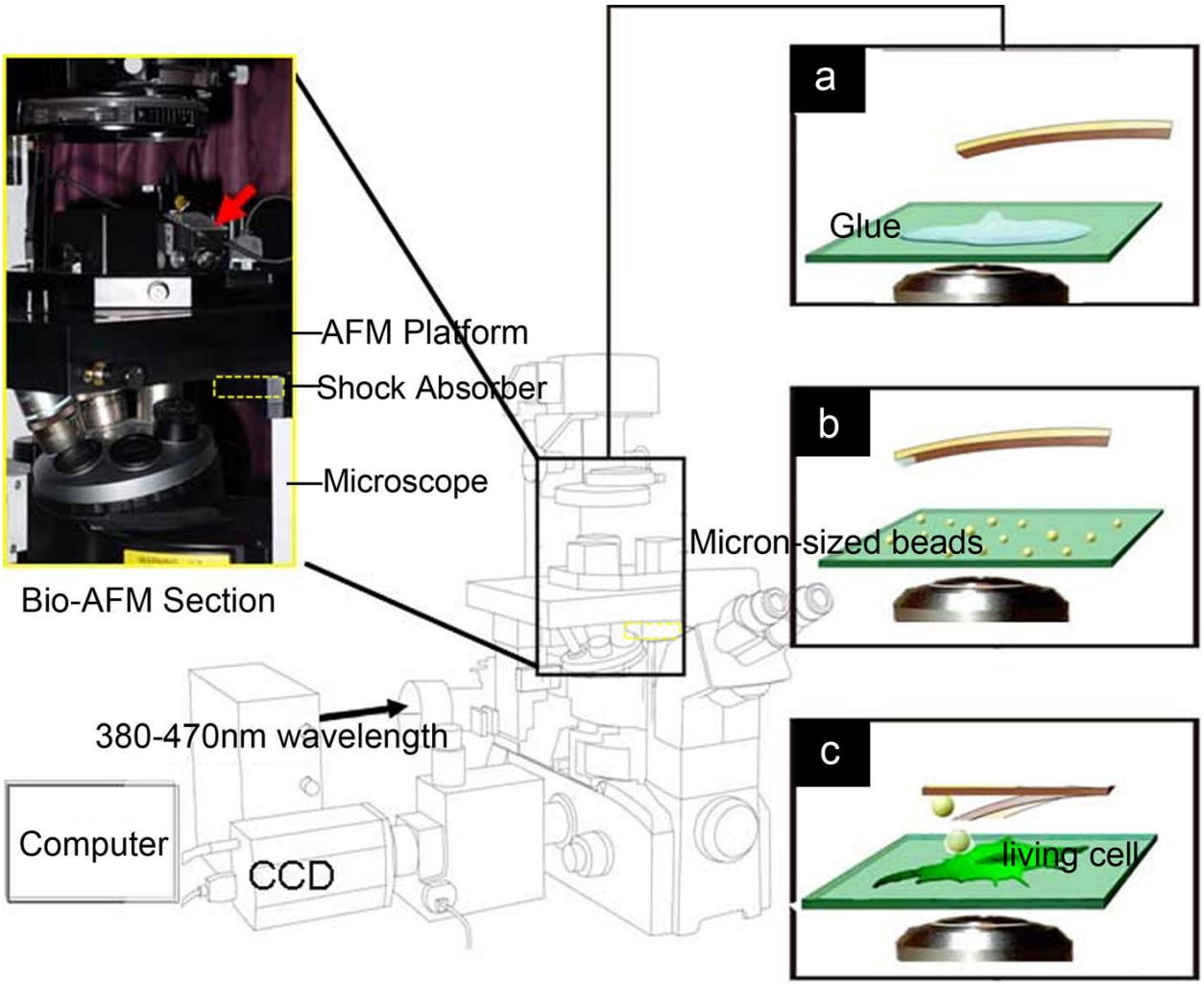

Figure 1. Schematic representation of a home-made BIO-AFM. Upper left insert figure: The zoomed-in picture of an MAC mode AFM section combined with an inverted microscope. The red arrow points to the AFM scanner. Insert figures right: a-c, The flow chart of attaching a micron-sized bead to the AFM cantilever probe and exerting nanoNewton forces onto the cells: (a) A cantilever probe is positioned close to the edge of glue. (b) The cantilever probe with glue is positioned close to the micron-sized beads. (c) The cantilever with a beads approaches to living cells. A 380-470 nm wavelength light was used to irradiate the cantilever via the lens system within the inverted microscope.

confluence exhibited the perspectives of histiotypic morphology of human PDLCs. Cells that had been passaged six times were used for experiments.

3.2. BIO-AFM combined system and imaging

The custom-made BIO-AFM combined system consists of an AFM section of magnetic AC mode (MAC mode), an inverted fluorescent microscope and a high-speed laser scanning confocal microscope (Figure 1 upper lift inset). The AFM instrument (5500 Agilent Co.) is placed on an inverted fluorescent microscope (Nikon, TE2000U) to achieve AFM and fluorescence images simultaneously. The fluorescent signal is detected by a charge-coupled device camera (Cascase 512B. Roper Scientific, Trenton, NJ), which is connected to a high-speed confocal device (CSU 10, Yokogawa). A Picoscan controller and a top MAC Mode control-box are used to control the scanner, acquire and convert analog signals to digital ones, and then transferred to the computer via a USB port. A large range scanner of $100\times100\mu m^2$ and a MAC mode nose are used for imaging. The cantilever, coated with magnetic materials, has a spring constant of $0.2Nm^{-1}$. The resonance frequency was chosen at 34-35kHz with a scan speed of 1Hz when imaging in the MAC mode was performed. Meanwhile, we also used the contact mode with a $0.08Nm^{-1}$ cantilever to image living PDLCs. In this case, noise induced by rotation of the spinning-disk's scanning head sometimes occured. In order to avoid this problem, a heavy platform on the AFM section was constructed. In addition, a shock absorber was connected to the AFM platform. The microscope (see the yellow square in Figure 1) was also designed to further eliminate the noise.

3.3. Attaching a micro-bead to the tipless AFM cantilevere and exerting nano-Newton forces onto the cells

In order to use the combined BIO-AFM system, a micron-sized glass bead was attached on a tipless cantilever as illustrated in Figure 1a-c. A slide with a small puddle of the UV-sensitive glue was placed on the sample stage. When monitored through the optical microscope, a cantilever was positioned close to the edge of the glue. Then the probe was approached automatically, controlled by the AFM device, and then slightly pushed into the glue. During this process, only the point of the probe touched the glue. Subsequently, the probe was withdrawn rapidly, dragging off the excess glue along the glass slide if needed. After this, the glue slide was replaced by another one with micron-sized glass beads. The probe was positioned on a top of a sphere glass and automatically approached to touch its foreside. A 380-470nm wavelength light irradiated the probe via the object lens for 30 seconds to solidify the glue. Then, the probe was again withdrawn. The slide was then replaced by the cell-culture dish to carry out the nanomechanical experiments.

A spreading-out and well-anchored cell was chosen and the probe was positioned above it. Then the cantilever approached again under the AFM operation. And the foreside of the glass bead was brought into contact with the cell to load a measurable compression force. The vertical loading force (Fn) was defined according to the formula:

$Fn = (\Delta V)KS$

Where ΔV = dsp - dvt, dsp is the deflection setpoint, and dvt is the vertical deflection. Both K (the constant force of the cantilever) and S (the sensitivity of the equipment) are constants.

3.4. Elasticity detection

The force volume (F-V) spectroscopy at designated points of every 8 points per scanning line on the living PDLCs' surface was conducted in contact mode. The AFM probe (ContAl, Budget Sensors) with a curvature diameter of 20-40nm was used. AFM images and force curves at regular intervals were obtained at the same time. An array of 32-by-32 force-distance curves was taken for per image. The scanning speed is at a rate of 1 Hz. The determination of the elastic modulus from the force curves was performed using Sneddon's modifications of the Hertz model for a purely elastic indentation in a flat and soft sample by a stiff cone (39, 40).

$$E = \frac{F(h)\cdot\pi\cdot(1-\nu_{Sample}^2)}{2\tan\alpha\cdot h^2}$$

Where E is the elastic modulus (Young's modulus), F is the applied loading force, h is the indentation depth (50 nm in this case), ν is Poisson's ratio, and α is the half angle of the AFM tip. Poisson's ratio was assumed to be 0.5 because the cell was considered incompressible at limited deflection of AFM tip.

3.5. Fluorescence imaging of nitric oxide integrated with force stimulation

To assess intracellular NO intensity, the cells were washed with a Mg^{2+}/Ca^{2+} buffer solution and incubated for 40 min in the buffer containing 5μM DAF-FM (Beyotime, City. China). DAF-FM is a cell permanent fluorescent fluorophore for the detection of intracellular NO at low concentrations. The cells were subsequently washed twice and incubated for a further 15 min in the buffer to remove any cell debris. The NO production was recorded via the high speed confocal laser scanning microscope with 488 nm excitation at 30 second intervals. The CSU-10 employs a spinning disc confocal system, achieving a maximum scanning speed of 360 frames/sec, which is faster than a standard confocal microscope that employs a pair of pinhole apertures. A Nikon Neoplan 100× oil immersion objective was used for imaging. The CCD with a high sensitivity (Cascade 512B) collected the signal at an exposure time of 500 milliseconds. During this process, one image of every 3 milliseconds in the spinning disc confocal system can't influence the data collection by the CCD. Images were acquired using the MetaMorph software (Universal Imaging, Dowington, PA). In the case, the temporal evolution of the fluorescence intensity at several locations could be assessed and was used to determine variations of the NO concentration.

The glass probe may lead to a slight deformation of the apical cell body, i.e, indentation, when it touches the cell membrane. Therefore, only the fluorescent signal from the cell bottom plane near the substrate was acquired by using the confocal microscope to avoid incorrect results. After 120s of data collection by the confocal microscope, the cantilever probe was approached toward the cell surface and kept contact with the cell membrane to exert a continuous compression force onto the cell.

The cells (n=4) treated by NO-synthase inhibitor-L-NMMA (100μM) were under parallel processing to confirm the process of NO response to mechanical stimulation as a negative control. Otherwise, the normal cells without the mechanical stimulation (n=4) were also imaged in parallel as the normal control.

We also selected a group of adjacent cells to carry out the nanomechanical stimulation and the NO responses among the adjacent cells were observed in real-time. In order to better monitor the detailed signal, the NO-related fluorescence was recorded at 5 second intervals from 0s to 1500s. The cantilever was approached toward the cell surface and kept contact with the cell membrane at 120s.

4. RESULTS

4.1. Cantilever probe with the attached micron-sized glass beads

As shown in Figure 2A, a glass bead with a diameter of 23μm can be perfectly anchored onto the foreside of a tipless cantilever, which can be seen clearly in the zoomed-in side-view (Figure 2B). Only the foreside of the probe holds a little glue which is enough to pick up the

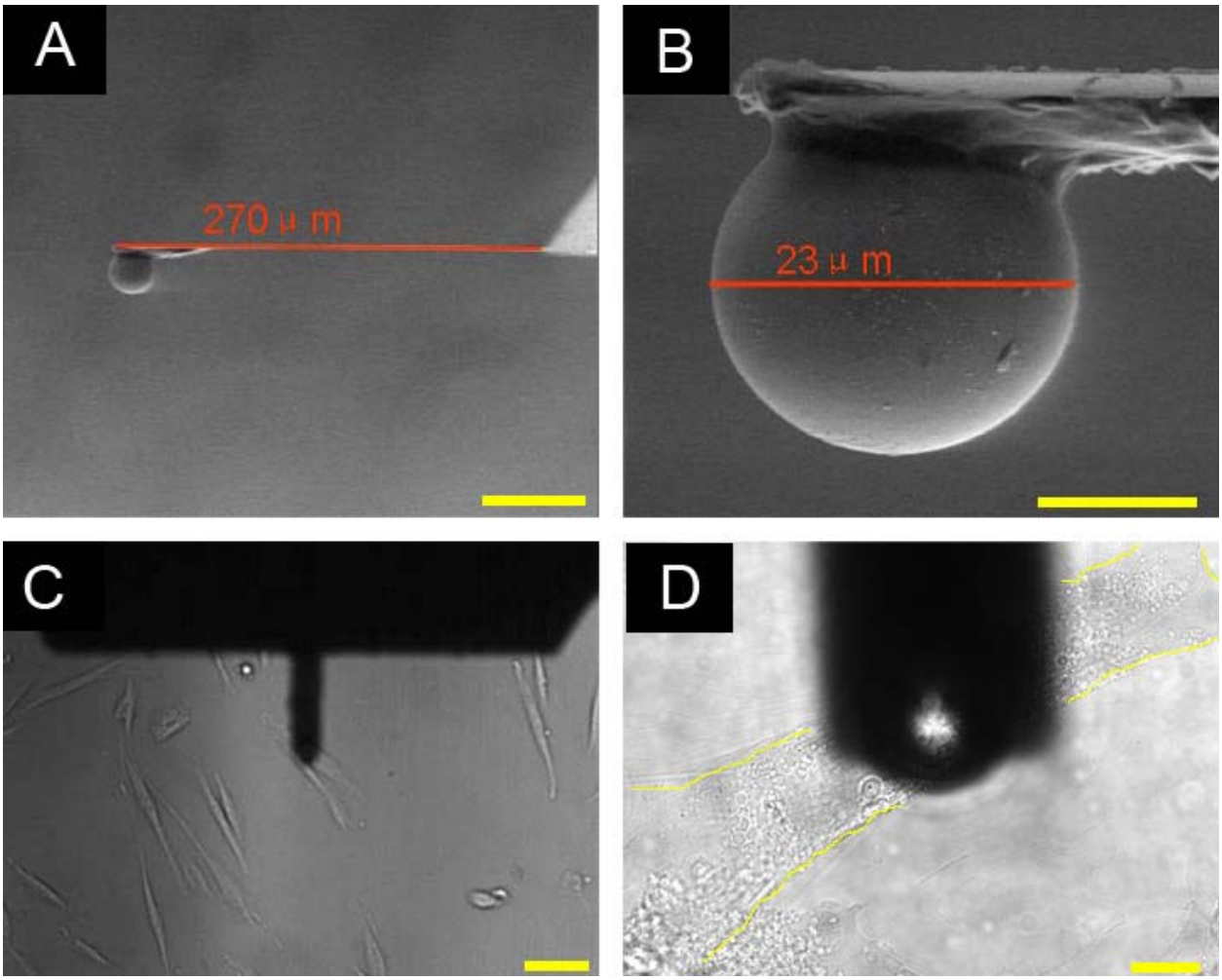

Figure 2. A, the environmental scanning electron microscopy image of a AFM cantilever probe with a 23 μm glass bead at the low vacuum of 0.75 Torr. B, The zoomed-in image of the probe in "A". C, The optical image of the probe positioned close to a living PDLC. D, The zoomed-in image of the probe in "C". The scale bar is 50 μm in A and C and 10 μm in B and D.

micro-bead (see Figure 2B) due to both the exact operation of the AFM device and instruction of optical microscope. The probe was then immerged into medium liquid to approach a cultured living PDLC (see Figure 2C). When monitored through the optical microscope, the probe can be accurately positioned at a given location, for example, the nuclear region or peripheral body (see Figure 2D). Subsequently, the AFM system controlled the probe to load a quantitative compressive force at nano-Newton levels onto the cells.

4.2. AFM Imaging of the PDLCs

One application of AFM is to acquire a high resolution image of living cells in their natural conditions. The cultured PDLCs have a spindle appearance as is shown in Figure 2C and D. Since the two scanning modes: the contact mode and the MAC mode rely on different mechanisms, the images obtained by each method demonstrate different characteristics of the PDLCs. In Figure 3A and B, the contact mode AFM images of cultured PDLCs, including topography image and deflection image, exhibit many strong cytoskeletal stress fibers (black arrows in Figure 3 A) that can be visualized beneath the cell surface, and appear to be organized along the axis of the cells. It is due to a large lateral force in contact mode that allows the cytoskeletal network beneath the membrane to be clearly imaged. These images can be further shown for contrast enhancement of the cytoskeleton features in the deflection image (black arrows in Figure 3B). These indicate that PDLCs have a strong capability of not only anchoring to the substrate but also withstanding the powerful lateral and compressive forces. By comparison, detailed surface information like the membrane protuberances (red arrows in Figure 3D) of a cell can be clearly resolved in both amplitude image and phase image in MAC mode. But the MAC mode imaging is easily disturbed by unstable surface ultrastructures (compare the red cycles in Figure 3A, B and those in Figure 3C, D) possibly due to the relative harder cantilever of 0.2N/m.

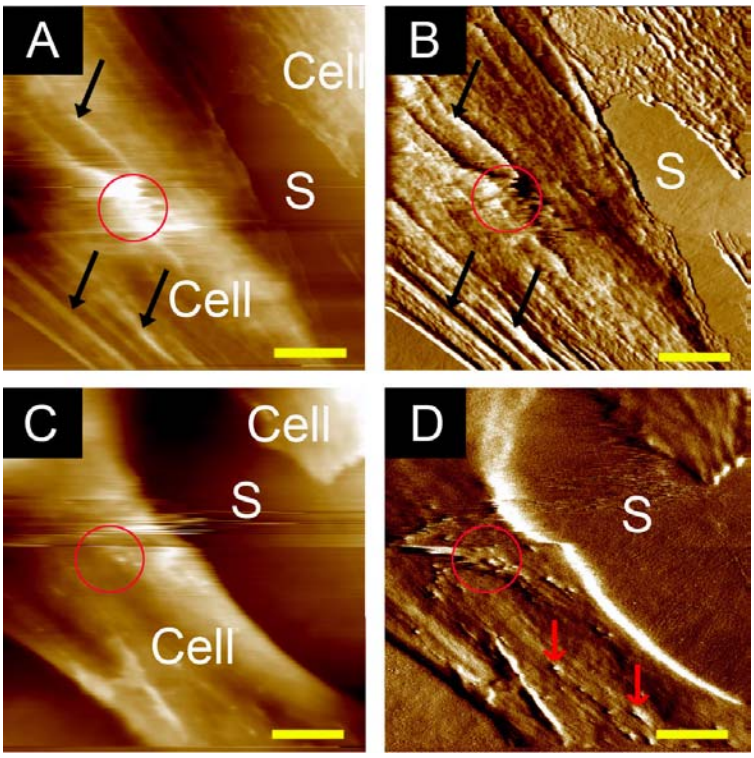

Figure 3. AFM image of living PDLCs. Contact mode AFM images: A, Topography image. Z range is 3000 nm. B, Deflection image. Z range is 5 nm. MAC mode AFM images of the same scanning region: C, Topography image. Z range is 2000 nm. D, Amplitude image. Z range is 20 nm. Red circles point out the unstable structures on the cell membrane. Black arrows show the typical stress fibers. Red arrows indicate the ultrastructures on the cell membrane. S represents the substrate of culture dish. The scale bar is 20 μm.

4.3. Elasticity detection of PDLCs

When the data points of F-V function were collected on a cell surface, the topography image (32×32 pixel Figure 4A) and corresponding stiffness image (Figure 4B) can be obtained simultaneously. The AFM probe tip at nanometer scale scans over the stressed fibers beneath the membrane (the black arrow in Figure 4A, B), as well as the membrane surface region between two fibers. Therefore, the data collected over the periphery body as well as the nuclear region of the cell shown in Figure 4A exhibited a distinct bi-peak distributing manner, which there are two peaks in the statistic histogram of Young's modulus (see Figure 4C). In the nuclear region, one peak was present at 168.7±2.3KPa and another peak was present at 798.1±21.21KPa. By comparison, in the periphery body, one peak was also present at 171.2±4.8KPa like that in the nuclear region and another peak was present at 625.0±29.1KPa, less than that in the nuclear region. These results strongly demonstrate that there are significant variations of the values of elastic modulus at different cell regions.

4.4. Nitric oxide production in the response of PDLCs to mechanical stimulation

In each experiment of mechanical stimulation, real-time fluorescence data were obtained. For all the cells stimulated by the compressive force, the responses of nitric oxide (NO) varied in magnitude throughout the cell were observed in the same manner. Figure 5A shows a typical NO-related fluorescent signal within one of the four cells we observed at successive time points from 0s to 1320s. We recorded the base line of fluorescent signal between 0s-120s. Then the AFM cantilever with a glass bead approached the cell at the time of 120s and was kept in contact with the body side of the cell as shown in Figure 5C (near the nuclear region). A persisted compressive force up to 1nN was loaded. In one such example, the fluorescence intensity started to increase within 60 seconds when the compressive force exerted on the cell (see the marker in Figure 5D), and remained gradually increasing until 900s. The NO fluorescent intensity began to increase in the center region near the indentation. Then the NO response spread out from the center region to the whole cell body step by step. The NO fluorescent intensity reached its peak at 900s and then started to decrease. The pool-like structures appeared step by step at the peripheral region (red square regions in Figure 5A) that seemed to secrete NO into the medium when NO response reaches the peak (clearly shown in Figure 5B, ref. zoomed-in pictures of the red squares in Figure 5A).

The normal control experiment exhibited a base line of the NO fluorescence intensity (see the black line in Figure 5D), indicating that the DAF-FM fluorophore did not be autoexcitated.

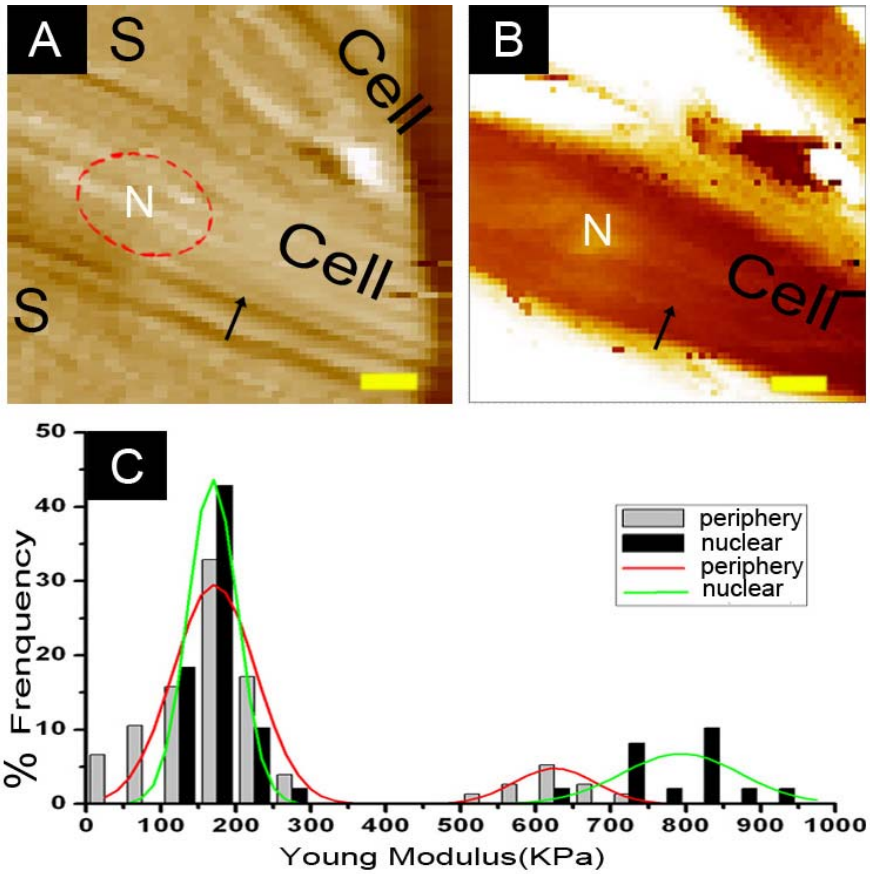

Figure 4. A, The topography image of a living PDLC with 32×32 pixels. Scanning range is 60×60μm. The red dashed circle represents the nuclear. S represents the substrate of culture dish. B, the corresponding stiffness image by F-V function. In general, the substrate is significantly stiffer than the cell. The nuclear region is relatively stiffer than the periphery region. C, Frequency histogram of the average Young's modulus values over the nuclear (black) and the periphery (grey) of the cell, respectively.

In the negative control experiment, the NO fluorescence intensity within the cells treated by NO-synthase inhibitor- L-NMMA represented a base line as similar as the normal control though a persisted force still exerted onto the cells (see the red line in Figure 5D).

In another interesting experiment, the NO responses among the adjacent cells were observed in details. Figure 6A shows three cells connected to each other. A same procedure like that in Figure 5A was carried out. A persisted compressive force was loaded at the side body of Cell 1. The changes in the NO-related fluorescence for Cell 1 exhibited the same case as the cell in Figure 5A. Interestingly, the Cell 2 and Cell 3 (only a part of their bodies can be shown in the view), also represented the same sequence but in a postponed time. The NO fluorescence intensities within Cell 2 and Cell 3 needed a longer time to reach their peaks. Meantime, the peaks of NO fluorescence intensities within Cell 2 and Cell 3 were relatively lower in comparison to Cell 1. Furthermore, a large pool-like structure was obviously presented at the peripheral region (red square regions in Figure 6A and zoomed-in pictures in Figure 6B) between Cell 1 and Cell 3 after the NO fluorescence intensity for Cell 1 reached the peak.

5. DISCUSSION

In the past decade, the combined BIO-AFM system (AFM and inverted fluorescent microscopy) has been developed into a practical integrated unit for biological applications (41, 42). Furthermore, in terms of simultaneous force measurement using fluorescence detection, there have been some previous suggestions for biological applications (43) and some review papers are also available (44, 45). Fluorescence microscopy based on the optical microscope is a routine cell imaging method and has been proved to be a powerful tool for selective and specific visualization of labeled molecules down to the single-molecule level (46), rendering it possible to follow cellular processes and monitor the dynamics of living cell components. In the described combined system, the AFM cantilever probe can be monitored to accurately touch a cell. In the meantime, the BIO-AFM system allows us not only to acquire a high resolution image of the living cell surface at the scale of nanometers, but also to

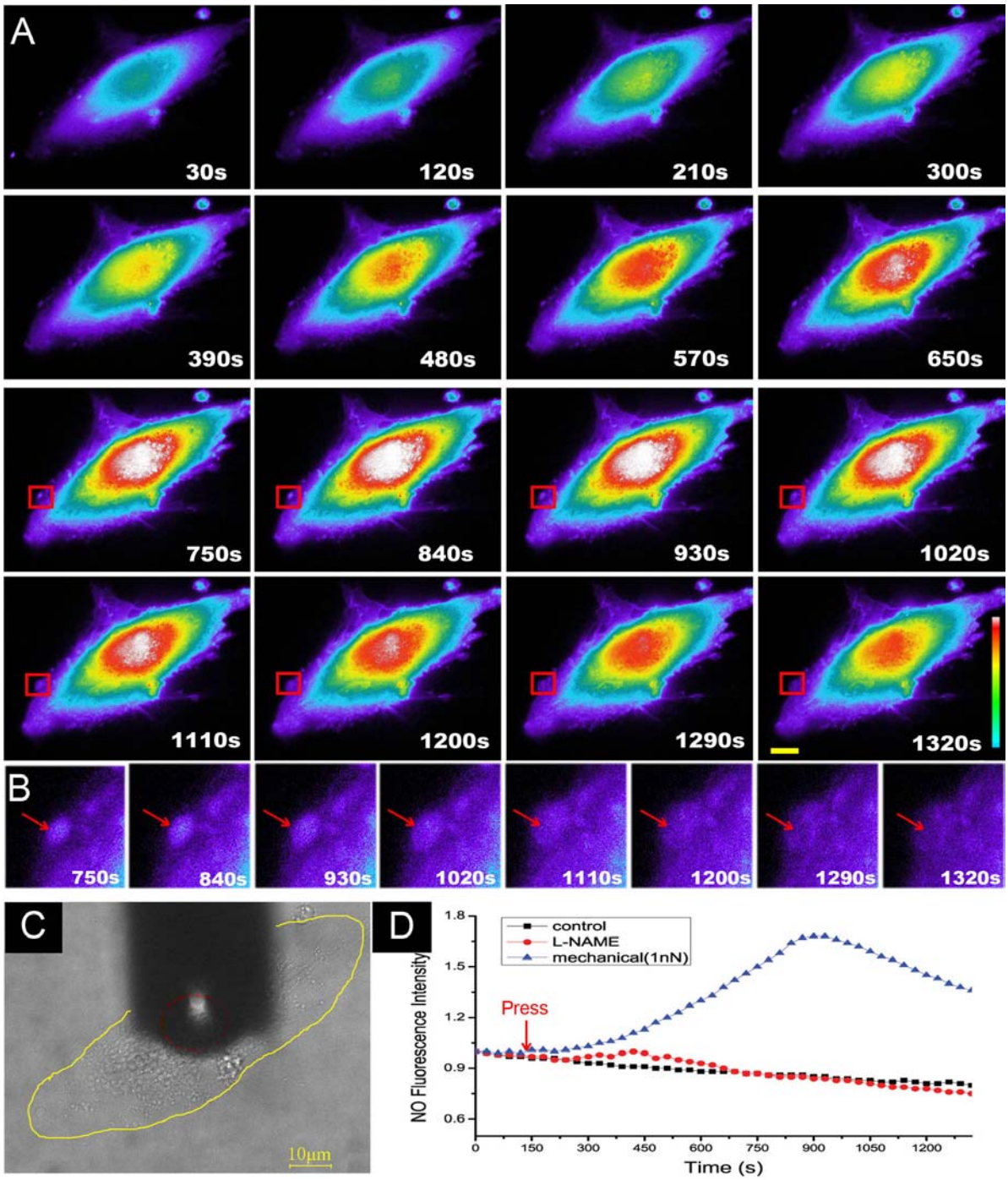

Figure 5. A, Time lapse images of intracellular NO intensity within a living PDLC stimulated by the compression force of 1 nN. We only showed the pictures from 30s to 1320s using a 90 second interval. The scale bar is 10μm. B, The corresponding zoomed-in pictures of the red square area in A. C, Imaging of optical microscope. The yellow solid line draws the outline of the cell and the red dashed circle represents the location of the glass bead. D, Typical curve diagram of the increased ratio of NO related fluorescent intensity within the cell stimulated by the compression force (blue line), a normal control cell (black line) and a negative control cell (red line), respectively, from 0s to 1320s.

simultaneously gain optical information within the cell body, especially the fluorescent signals (47). Regarding our custom-made combined system, both the MAC mode AFM and high speed confocal device are involved. The MAC mode AFM allows us to better perform imaging at high resolution in liquid environments as mentioned previously (48). In addition, the high-speed confocal device improves time-resolved recording of fluorescent trail. Therefore, this

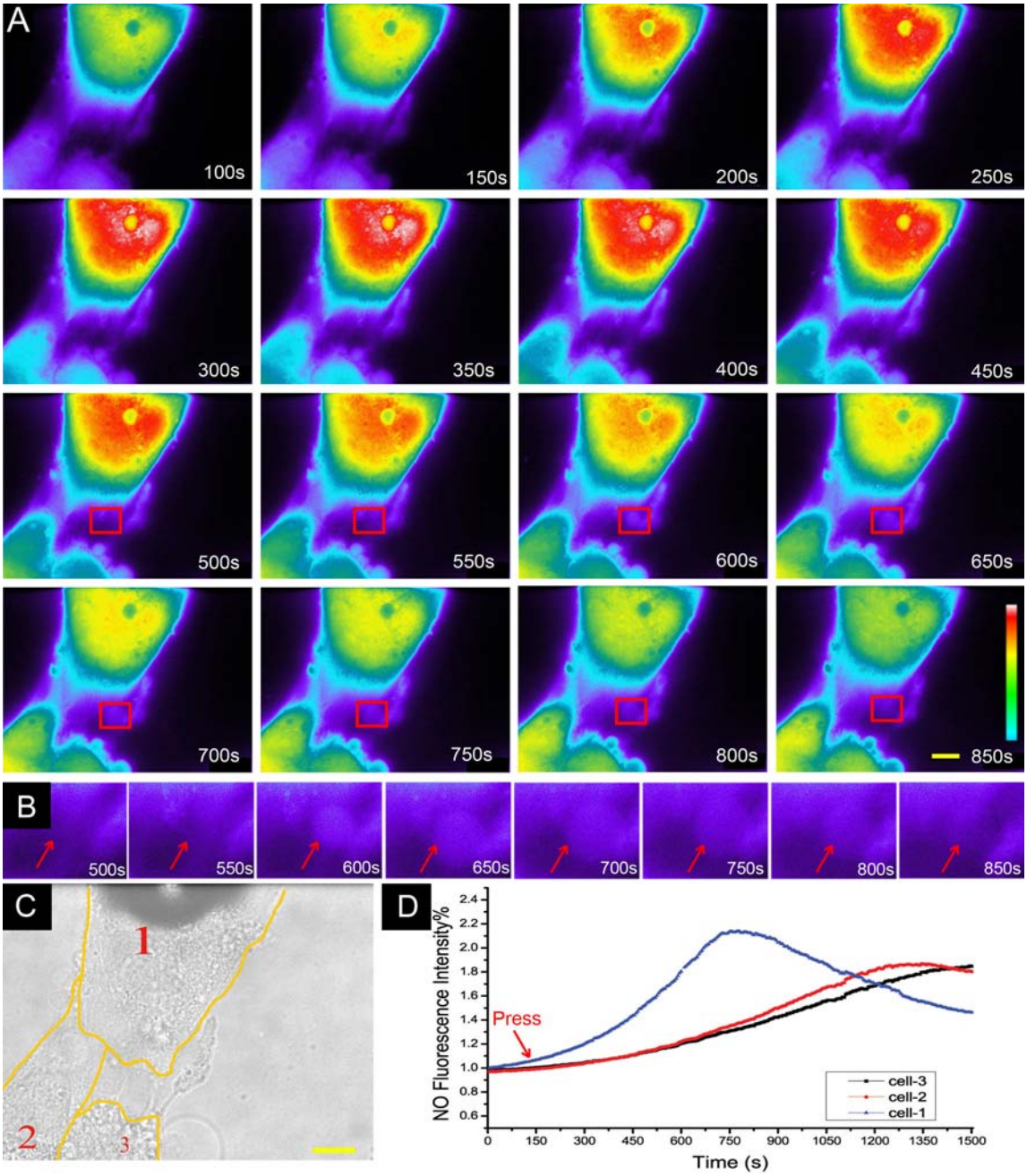

Figure 6. A, Time lapse images of intracellular NO intensity within three adjacent cells. We only showed the pictures from 100s to 850s using a 50 second interval. The scale bar is 10μm. B, The corresponding zoomed-in pictures of the red square area in A. C, Imaging of optical microscope. The yellow solid line draws the outline of the Cell 1, Cell 2 and Cell 3, respectively. The glass bead can be positioned clearly in this image. The scale bar is 10μm. D, Typical curve diagram of the increased ratio of NO related fluorescence intensity of the three cells in the picture, i.e., the blue line for Cell 1, the red one for Cell 2 and black one for Cell 3, respectively, from 0s to 1500s.

manner of the combined system is better adapted to an integrative view of biomedicine research.

In this study, the high resolution imaging of living cultured PDLCs was achieved in the contact mode for the first time. The result indicates that the PDLCs hold a strong network of stress fibers allowing them to tolerate strong external forces, and connecting to the cementum of the dental root and alveolar bones. MAC mode AFM was also successfully applied to image the subtle ultrastructures both on the living PDLCs' surface and beneath their apical membrane due to the deformation of cell membrane. It is

expected to obtain a deeper understanding of structural changes in cell functions.

Furthermore, the main application of BIO-AFM is the study of mechanotransduction (49, 50). Besides unmodified AFM probes, the probes modified by different microscale spheres, for example glass-beads, were employed to precisely exert the global force to an individual cell.

With the former techniques, the glue (usually epoxy resin) is used to attach a micron-sized bead to the AFM probe tip. A tip modified with a sphere which has a smooth surface and diameter of >1 μm yields advantages over a bare tip. The sphere has a well-defined geometry that may better facilitate the data interpretation, so more accurate information can thus be derived from force curves (51, 52). A particle bigger than 1 μm can easily be observed by an optical microscope, therefore, besides the three-dimensional micromanipulator, it is a common tool used for attaching a micron-sized bead.

The dual-wire technique, originally reported by Ducker *et al* in their classic papers (51, 53) is the most popular method for the attachment of micron-sized beads. This technique is especially suitable for dealing with tipless cantilevers, because the flat end facilitates the application of the glue and setting the bead in place.

For another technique, the cantilever is moved around either by a 3D manipulator or on an AFM head, instead of moving wires (54-55). However, it is still difficult to modify micron-sized glass beads onto the AFM cantilevers. This is presumably due to three factors that are difficult to control: (a) the contact of a small amount of glue with a cantilever, (b) the contact of the glass bead sphere with the glued cantilever, and (c) the solidification time of the glue. In conclusion, the major disadvantage of the described techniques is that some special instruments have to be used, such as a micromanipulator equipped with a heater and glass needles

In order to overcome these difficulties, we used a simple and controllable method to adhere micron-sized beads on the foreside of AFM cantilevers by the BIO-AFM system, thus establishing a systematic and convenient tool for the mechano-transduction study at single cell levels. In this technique, the AFM and appropriate light source are required. The AFM device automatically controls the cantilever under the monitoring of optical microscope during the whole process. Meantime, the light-sensitive polymer was selected as the glue and the light source of the inverted microscope was employed to solidify the glue. The results strongly reveal that both the AFM cantilevers and the beads are kept in good shape and bonded firmly. Employing the loading system based on AFM to exert precise compressive forces, we can easily collect the fluorescent signals to achieve the nano-mechanical research of living PDLCs at the single cell level.

Among various external mechanical forces applied to cells, the compressive force is the main stress, which is resisted through cell adhesions by underlying extracellular matrix (ECM), neighboring cells, and especially internal stress fibers. Some genes, like RhoE and RGS2, which are major regulators of cytoskeleton dynamics, were proved to be differentially expressed by mechanical force loading (24). The contact mode AFM images in our studies also confirmed that there are abundant networks of stress fibers within the PDLCs. The F-V function data carried out point by point also show a discrete manner that is presumed to be relevant to the distribution of stress fibers, leading to the heterogeneity of mechanical properties of cells. The high elasticity values at the indentation site indicate that the cytoskeleton fibers were indented. Because the cell holds a strong and compact stress fiber network to protect the nuclear structure, the F-V function data represent the distinct bi-peak distributing curve of elasticity over the nucleus. On the contrary, there are relative infirm networks of stress fibers within the peripheral region of cells, where most of the lower elastic modulus are present.

Furthermore, different types of cells also represent variations of the values of elastic modulus. Mathur *et al* (56) reported that the elastic modulus value of human umbilical vein endothelial cells was 7.22±0.46KPa over the nucleus, and 2.97±0.79KPa over the central body in proximity to the nucleus, and a lower magnitude of 1.27±0.36KPa on the peripheral body near the cell edge. However, the cell central body of bovine pulmonary artery endothelial cells were two- to three-fold softer than the cell periphery, as reported by Costa and Yin (57). The corresponding study on cardiomyocytes also revealed that cells were softer at the nuclear region, and become stiffer toward the periphery (58). After mapping according to the Young's modulus across the living chicken cardiocytes, Hofmann *et al* (59) stated that the stress fibers were characterized by the presence of areas with a stiffness of 100–200kPa embedded in softer parts of the cell with elastic modulus values between 5 and 30kPa. The elasticity mapping images of living astrocytes (glial cells of nerve tissue) in the previous literature (60) showed that cell membrane above the nucleus was softer (2–3kPa) than the surroundings, and that the cell membrane above F-actin network structures was stiffer (10–20kPa) than the surroundings.

In comparison to varied types of cells, the PDLCs exhibit a high elastic modulus value in proximity to the cardiocytes. It possibly agrees with the PDLCs functions as a mechanical responder and regulators between the cementum of the dental root and alveolar bones. But the question is how the living PDLCs respond to an external compressive force. In the present study, we observed the NO response of living single cell to a nano-Newton loading force.

NO is a small, diatomic gas and a radical and, therefore, a highly reactive molecule transferring biochemical signals, which result in a wide spectrum of effects on different biological systems (61, 62). It also acts as an important hemodynamic regulator (63), as well as a widely distributed chemical second messenger (64) in both

intracellular and intercellular actions. It activates guanyl cyclase enzyme and modulates actions of several bioactive peptides as well as neuronal transmitters (61, 65).

NO also plays other roles in cells, such as in isoprenylation (geranylgeranylation) of the Rho GTPase that activates Rho-PK, involving the activation of the bone morphogenetic protein (BMP)-2/Cbfa1-Runx-2 cycle (65, 66). The broad ranging actions of NO are determined largely by both the site and rate of NO synthesis, the quantity generated, and the nature of the environment into which it is released. The reactivity of NO is affected by the presence of reactive oxygen intermediates and the activity of antioxidant defense systems (67, 68). NO is enzymatically produced by oxidation and cleavage of the amino-terminal nitrogen atom of amino acid L-arginine. The reaction is dependent on electrons donated by the cofactor NADPH that requires oxygen, and it yields L-citrulline as a coproduct (69).

In a previous study, the characteristic NO responses of single osteoblasts, another type of compressive force-sensitive cell, to the indentation using AFM tips were observed and described (70). When the periodic indentation with peak forces ranging from 17 to 50nN were loaded, the indented osteoblasts stimulated four distinct responses: (a) a rapid and sustained diffusion of NO from the perinuclear region, (b) diffusion of NO from localized pools throughout the osteoblasts, (c) an initial increase and subsequent drop in intracellular NO, and (d) retraction of the indented osteoblast morphology with no NO response. In our present study, the similar response of NO were observed for the PDLCs when a compressive force up to 1nN was loaded by using the AFM probe with a micron-sized bead. A rapid and sustained diffusion of NO from the central region to the peripheral region were observed though the touched region was not located at the central region. The pool-like structures in the peripheral region of the PDLCs similar to the osteoblasts also appeared. Furthermore, the same manner of an initial increase and subsequent drop in intracellular NO was present in the PDLCs. It can be presumed that it performed a self-defense mechanism for the stimulation from a persisted force. We are unfamiliar with any mechanism that would degrade NO within the cell, so we suggest that this depletion of intracellular NO is because NO rapidly diffuses through the cell membrane into the medium. For example (Figure 5A), the initial increase in NO was accompanied by the emergence of bulges in the membrane that diffused outward. Indeed, NO is not stored within the cell, and may be released after reaching high concentrations. The results of the intercellular NO responses strongly confirm that NO may diffuse from the stimulated cell to its adjacent cells either via the medium or directly through the connected cell membrane, contributing the NO responses within these cells.

6. CONCLUSION

AFM-probing of whole cells is an effective method for studying membrane and sub-membrane cell structures as well as their elasticity properties. When the AFM is integrated with fluorescence imaging, the BIO-AFM system may act as a powerful technique in life science. Our single-cell nano-mechanical approach based on the BIO-AFM system is a significant advance in elucidating the magnitude, location, time scale, and biomolecular mechanisms underlying force-sensitive cell mechano-transduction.

In this article, we focus on the application of a single-cell nano-mechanical approach to study the mechanical mechanisms of PDLCs. It is known that mechanical stress loaded onto a tooth is transduced to the periodontal ligament. The cells in the periodontal ligament respond to mechanical stress by signaling to surrounding cells to regulate resorption and formation of bone matrix. We believe that more extensive studies on mechano-transduction within the PDLCs will add new information about the key mechanisms in physiological and pathological processes of tooth development, root resorption, and improve orthodontic treatment.

7. ACKNOWLEDGMENT

Liang Shi, Shenggen Shi & Jing Li equally contributed to this work. The authors were supported by the MOST Project 973 (Nos. 2009CB930200 and 2006CB705600) and the National Nature Science Foundation of China (No. 90709054 and No. 30872911).

8. REFERENCES

1.Masako Tamadaa, Michael Sheetz and Yasuhiro Sawada: Activation of a signaling cascade by cytoskeleton stretch. *Dev Cell* 7, 709-718 (2004)

2. Nikola Kojić, Miloš Kojić and Daniel Tschumperlin. Computational modeling of extracellular mechanotransduction. *Biophys J* 90, 4261-70 (2006)

3. Wayne Orr, Brian Helmke, Brett Blackman and Martin Schwartz: Mechanisms of mechanotransduction. *Dev Cell* 10, 11-20 (2006)

4. Frederick Sachs and Catherine Morris: Mechanosensitive ion channels in nonspecialized cells. *Rev Physiol Biochem Pharmacol* 132, 1-77 (1998)

5. Albert Banes, Mari Tsuzaki, Juro Yamamoto, Thomas Fischer, Brian Brigman, Thomas Brown and Larry Miller. Mechanoreceptionat the cellular level: the detection, interpretation, and diversity of responses to mechanical signals. *Biochem Cell Biol* 73, 349–365 (1995)

6. Adel Malek and Seigo Izumo: Mechanism of endothelial cell shape change and cytoskeletal remodeling in response to fluid shear stress. *J Cell Sci* 109, 713-26 (1996)

7. Kevin Ko and Christopher McCulloch: Partners in protection: interdependence of cytoskeleton and plasma membrane in adaptations to applied forces. *J Membr Biol* 174, 85-95 (2000)

8. Paul Janmey: The cytoskeleton and cell signaling: component localization and mechanical coupling. *Physiol Rev* 78, 763-81 (1998)

9. Ning Wang. Mechanical interactions among cytoskeletal filaments. *Hypertension* 32, 162–165, (1998)

10. Christian Rotsch and Manfred Radmacher: Drug-induced changes of cytoskeletal structure and mechanics in fibroblasts: an atomic force microscopy study. *Biophys J* 78, 520-35 (2000)

11. Predrag Lekic and Christopher McCulloch. Periodontal ligament cell populations: The central role of fibroblasts in creating a unique tissue. *Anat Rec* 245, 321–341 (1996)

12. David Mitchell and John West: Attempted orthodontic movement in the presence of suspected ankylosis. *Am J Orthod* 68, 404-11 (1975)

13. Najat Alhashimi, Lars Frithiof, Pongsri Brudvik and Moiz Bakhiet: Orthodontic tooth movement and de novo synthesis of proinflammatory cytokines. *Am J Orthod Dentofacial Orthop* 119, 307-12 (2001)

14. Noriyoshi Shimizu, T. Goseki, Masaru Yamaguchi, T. Iwasawa, H. Takiguchi and Yoshimitsu Abiko. *In vitro* Cellular Aging Stimulates Interleukin-1β Production in Stretched Human Periodontal-ligament-derived Cells. *J Dent Res* 76, 1367-1375 (1997□

15. Laura Iwasaki, Jason Haack, Jeffrey Nickel, Richard Reinhardt and Thomas Petro: Human interleukin-1 beta and interleukin-1 receptor antagonist secretion and velocity of tooth movement. *Arch Oral Biol* 46, 185-9 (2001)

16. Ping Long, Feng Liu, Nicholas Piesco, Rashmi Kapur and Sudha Agarwal: Signaling by mechanical strain involves transcriptional regulation of proinflammatory genes in human periodontal ligament cells *in vitro. Bone* 30, 547-52 (2002)

17. Anne-Laure Bolcato-Bellemin, René Elkaim, A. Abehsera, J. L. Fausser, Youssef Haikel and Henri Tenenbaum: Expression of mRNAs encoding for alpha and beta integrin subunits, MMPs, and TIMPs in stretched human periodontal ligament and gingival fibroblasts. *J Dent Res* 79, 1712-6 (2000)

18. Shigeru Miuraa, Masaru Yamaguchia, Noriyoshi Shimizuc and Yoshimitsu Abiko: Mechanical stress enhances expression and production of plasminogen activator in aging human periodontal ligament cells. *Mech Ageing Dev* 112, 217-31 (2000)

19. Noriyoshi Shimizu, Y. Ozawa, Masaru Yamaguchi, T. Goseki, Kimimaro Ohzeki and Yoshimitsu Abiko: Induction of COX-2 expression by mechanical tension force in human periodontal ligament cells. *J Periodontol* 69, 670-7 (1998)

20. Kimimaro Ohzeki, Masaru Yamaguchi, Noriyoshi Shimizu and Yoshimitsu Abiko: Effect of cellular aging on the induction of cyclooxygenase-2 by mechanical stress in human periodontal ligament cells. *Mech Ageing Dev* 108, 151-63 (1999)

21. Masaru Yamaguchia, Noriyoshi Shimizu, Yasuko Shibata and Yoshimitsu Abiko: Effects of different magnitudes of tension-force on alkaline phosphatase activity in periodontal ligament cells. *J Dent Res* 75, 889-94 (1996)

22. Masahiro Nakagawa, Toshio Kukita, Akihiko Nakasima1 and Kojiro Kurisu. Expression of the type I collagen gene in rat periodontal ligament during tooth movement as revealed by *in situ* hybridization. *Arch Oral Biol* 39, 289-294 (1994)

23. N. Matsuda, K. Yokoyama, S. Takeshita and M. Watanabe: Role of epidermal growth factor and its receptor in mechanical stress-induced differentiation of human periodontal ligament cells *in vitro*. *Arch Oral Biol* 43, 987-97 (1998)

24. Rui Araujo, Yasuo Oba and Keiji Moriyama: Identification of genes related to mechanical stress in human periodontal ligament cells using microarray analysis. *J Periodont Res* 42, 15-22, 2007□

25. Hiroyuki Kanzaki, Mirei Chiba,Yoshinobu Shimizu and Hideo Mitani: Periodontal ligament cells under mechanical stress induce osteoclastogenesis by receptor cctivator of nuclear factor κB ligand up-regulation via prostaglandin E2 synthesis. *J Bone Miner Res* 17, 210-20 (2002)

26. Shenling Xia and Jack Ferrier: Propagation of a calcium pulse between osteoblastic cells. *Biochem Biophys Res Commun* 186, 1212-9 (1992)

27. Niklas Jørgensen, Steven Geist, Roberto Civitelli and Thomas Steinberg: ATP- and gap junction-dependent intercellular calcium signaling in osteoblastic cells. *J Cell Biol* 139, 497-506 (1997)

28. Michael Glogauer, Jack Ferrier and Christopher McCulloch: Magnetic fields applied to collagen-coated ferric oxide beads induce stretch-activated Ca2+ flux in fibroblasts. *Am J Physiol Cell Physiol* 269, C1093-C1104 (1995)

29. Juliet Lee, Akira Ishihara, Gerry Oxford, Barry Johnson and Ken Jacobson: Regulation of cell movement is mediated by stretch-activated calcium channels. *Nature* 400, 382-386 (1999)

30. Manfred Radmacher: Measuring the elastic properties of biological samples with the AFM. *IEEE Eng Med Biol Mag* 16, 47-57 (1997)

31. Philip Haydon, Raj Lartius, Vladimir Parpura and Silvio Marchese-Ragona: Membrane deformation of living

glial cells using atomic force microscopy. *J Microsc* 182, 114–120 (1996)

32. Guillaume Charras, Petri Lehenkari and Michael Horton. Atomic force microscopy can be used to mechanically stimulate osteoblasts and evaluate cellular strain distributions. *Ultramicroscopy* 86, 85–95 (2001)

33. Gerd Binnig, Calvin Quate and Christoph Gerber: Atomic force microscope. *Phys Rev Lett* 56, 930-933 (1986)

34. Youdong Mao, Quanmei Sun, Xiufeng Wang, Qi Ouyang, Li Han, Lei Jiang and Dong Han: *In vivo* nanomechanical imaging of blood-vessel tissues directly in living mammals using atomic force microscopy*In vivo* nanomechanical imaging of blood-vessel tissues directly in living mammals using atomic force microscopy. *Appl Phys Lett* 95, 013704 (2009)

35. Christian Rotscha and Manfred Radmacher: Drug-induced changes of cytoskeletal structure and mechanics in fibroblasts: an atomic force microscopy study. *Biophys J* 78, 520-35 (2000)

36. Andrew Pelling, Sadaf Sehati, Edith Gralla, Joan Valentine and James Gimzewski: Local nanomechanical motion of the cell wall of Saccharomyces cerevisiae. *Science* 305, 1147-50 (2004)

37. Martha Somerman, S. Y. Archer, G. R. Imm and Ruth Foster: A comparative study of human periodontal ligament cells and gingival fibroblasts *in vitro*. *J Dent Res* 67, 66-70 (1988)

38. Masaru Yamaguchi, Noriyoshi Shimizu, Yasuko Shibata and Yoshimitsu Abiko: Effects of different magnitudes of tension-force on alkaline phosphatase activity in periodontal ligament cells. *J Dent Res* 75, 889-94 (1996)

39. Anshu Bagga Mathura, George Truskeya and Monty Reichert: Atomic force and total internal reflection fluorescence microscopy for the study of force transmission in endothelial cells. *Biophys J* 78, 1725-35 (2000)

40. Valérie Laurent, Sandor Kasas, Alexandre Yersin, Tilman Schäffer, Stefan Catsicas, Giovanni Dietler, Alexander Verkhovsky and Jean-Jacques Meister: Gradient of rigidity in the lamellipodia of migrating cells revealed by atomic force microscopy. *Biophys J* 89, 667-75 (2005)

41. Constant Putman, Bart Grooth, Niek Hulst and Jan Greve. A theoretical comparison between interferometric and optical beam deflection technique for the measurement of cantilever displacement in AFM. *Ultramicroscopy* 42-44, 1509-1513 (1992)

42. Mike Horton, Guillaume Charras, Christoph Ballestrem and Petri Lehenkari: Integration of atomic force and confocal microscopy. *Single Mol* 1, 135-137 (2000)

43. Takashi Kodama, Hiroyuki Ohtani, Hideo Arakawa and Atsushi Ikai: Mechanical perturbation-induced fluorescence change of green fluorescent protein. *Appl Phys Lett* 86, 043901 (2005)

44. John Oreopoulos and Christopher Yip: Combined scanning probe and total internal reflection fluorescence microscopy. *Methods* 46, 2-10 (2008)

45. Sandor Kasas and Giovanni Dietler: Probing nanomechanical properties from biomolecules to living cells. *Pflugers Arch* 456, 13-27 (2008)

46. Peter Hinterdorfer, Gerhard Schütz, Ferry Kienberger and Hansgerog Schindler: Detection and characterization of single biomolecules at surfaces. *Rev Mol Biotechnol* 82, 25-35 (2001)

47. Long Chen, Weiguo Chu, Yonggang Xu, Peipei Chen, Fulong Liao, Quanmei Sun and Dong Han: Time-series investigation of fused vesicles in microvessel endothelial cells with atomic force microscopy. *Microsc Res Tech (*2009)

48. Guanglu Ge, Dong Han, Danying Lin, Weiguo Chu, Yunxu Sun, Lei Jiang, Wanyun Ma and Chen Wang: MAC mode atomic force microscopy studies of living samples, ranging from cells to fresh tissue. *Ultramicroscopy* 107, 299-307 (2007)

49. Josef Madl, Sebastian Rhode, Herbert Stangl, Hannes Stockinger, Peter Hinterdorfer, Gerhard J. Schütz and Gerald Kada: A combined optical and atomic force microscope for live cell investigations. *Ultramicroscopy* 106, 645-51 (2006)

50. Andreea Trache and Gerald Meininger: Atomic force-multi-optical imaging integrated microscope for monitoring molecular dynamics in live cells. *J Biomed Opt* 10, 064023 (2005)

51. William Ducker, Tim Senden and Richard Pashley: Direct measurement of colloidal forces using an atomic force microscope. *Nature* 353, 239-241 (1991)

52. Hans-Jürgen Butt: Measuring electrostatic, van der Waals, and hydration forces in electrolyte solutions with an atomic force microscope. *Biophys J* 60, 1438-1444 (1991)

53. William Ducker, Tim Senden and Richard Pashley: Measurement of forces in liquids using a force microscope. *Langmuir* 8, 1831-1836 (1992)

54. Roberto Raiteri, Markus Preuss, Massimo Grattarola and Hans-Jürgen Butt. Preliminary results on the electrostatic double-layer force between two surfaces with high surface potentials. *Colloid and Surface A* 136, 191-197 (1998)

55. Richard Bowen, Nidal Hilal, Robert Lovitt and Chris Wright. An atomic force microscopy study of the adhesion

of a silica sphere to a silica surface-effects of surface cleaning. *Colloid and Surface A* 157, 117-125 (1999)

56. Anshu Mathur, Amy Collinsworth, William Reichert, William Kraus and George Truskey: Endothelial, cardiac muscle and skeletal muscle exhibit different viscous and elastic properties as determined by atomic force microscopy. *J Biomech* 34, 1545–1553 (2001)

57. Kevin Costa and Frank Yin. Analysis of indentation: implications implications for measuring mechanical properties with atomicforce microscopy. *J Biomech Eng* 121, 462–471 (1999)

58. Sanjeev Shroff, Donald Saner and Ratneshwar Lal: Dynamic micromechanical properties of cultured rat atrial myocytes measured by atomic force microscopy. *Am J Physiol* 269, C286-292 (1995)

59. Ulrich Hofmann, Christian Rotsch, Wolfgang Parak and Manfred Radmacher: Investigating the cytoskeleton of chicken cardiocytes with the atomic force microscope. *J Struct Biol* 119, 84-91 (1997)

60. Yukako Yamane, Hatsuki Shiga, Hisashi Haga, Kazushige Kawabata, Kazuhiro Abe and Etsuro Ito: Quantitative analyses of topography and elasticity of living and fixed astrocytes. *J Electron Microsc* 49, 463-71 (2000)

61. Salvador Moncada, Richard Palmer and Annie Higgs: Nitric oxide: physiology, pathophysiology, and pharmacology. *Pharmacol Rev* 43, 109-42 (1991)

62. Louis Ignarro, Georgette Buga, Keith Wood, Russell Byrns and Gautam Chaudhuri: Endothelium-derived relaxing factor produced and released from artery and vein is nitric oxide. *Proc Nati Acad Sci* 84 (24), 9265-9269 (1987□

63. R. M. Palmer, A. G. Ferrige and S. Moncada: Nitric oxide release accounts for the biological activity of endothelium-derived relaxing factor. *Nature* 327,524-6 (1987)

64. Charles Lowenstein, Jay Dinerman and Solomon Snyder: Nitric oxide: a physiologic messenger. *Ann Intern Med* 120, 227-37 (1994)

65. Sunil Wimalawansa: Rationale for using nitric oxide donor therapy for prevention of bone loss and treatment of osteoporosis in humans. *Ann NY Acad Sci* 1117, 283-97 (2007)

66. Ronald Margolis and Sunil Wimalawansa: Novel targets and therapeutics for bone loss. *Ann N Y Acad Sci* 1068, 402-9 (2006)

67. Salvador Moncada and Annie Higgs: The L-arginine-nitric oxide pathway. *N Engl J Med* 329, 2002-12 (1993)

68. Steven Gross and Michael Wolin: Nitric oxide: pathophysiological mechanisms. *Ann Rev Physiol* 57, 737-69 (1995)

69. Sunil Wimalawansa: Nitric oxide: new evidence for novel therapeutic indications. *Expert Opin Pharmacother* 9, 1935-54 (2008)

70. James McGarry, Paula Maguire, Veronica Campbell, Brian Connell, Patrick Prendergast and Suzanne Jarvis: Stimulation of nitric oxide mechanotransduction in single osteoblasts using atomic force microscopy. *J ORTHOP Res* 26, 513-521 (2007)

Abbreviations: AFM: atomic force microscope; PDLCs: periodontal ligament cells; NO: nitric oxide; RANKL: receptor activator nuclear factor kB ligand; PGE2: prostaglandin E2; F-V: force volume

Key Words: Atomic force microscopy, elastic modulus, fluorescence imaging, nitric oxide, periodontal ligament cells, mechanotransduction

Send correspondence to: Dong Han, Addresses: No.11 Beiyitiao Zhongguancun Beijing China 100190, Tel:86-10-82545568, Fax: 86-10-62656765, E-mail: dhan@nanoctr.cn

http://www.bioscience.org/current/vol2E.htm